

Electronic Supplementary Information for

Topological analysis and control of post-synthetic metalation sites in Zr-based Metal-organic Frameworks

Pol Gimeno-Fonquernie,^a Jorge Albalad,^a Jason R. Price,^b Witold M. Bloch,^c Jack Evans,^{a*} Christian J. Doonan^{a*} and Christopher J. Sumby^{a*}

^a Centre for Advanced Nanomaterials and Department of Chemistry, School of Physics, Chemistry and Earth Sciences, The University of Adelaide, Adelaide, SA 5000, Australia.

Email: j.evans@adelaide.edu.au; christian.doonan@adelaide.edu.au; christopher.sumby@adelaide.edu.au

^b ANSTO Melbourne, The Australian Synchrotron, 800 Blackburn Rd, Clayton, Vic 3168, Australia.

^c College of Science & Engineering, Flinders University, Sturt Road, Bedford Park, SA 5042, Australia.

Table of Contents

S1.	Main text supporting data.....	3
S2.	Fourier Transform Infrared Spectroscopy (FTIR) spectra.....	18
S3.	Adsorption experiments	19
S4.	Single crystal X-ray crystallography	22
	S4.1. Specific Data and Refinement Details	22
	S4.2. Thermal ellipsoid plots for all structures at the 50% probability level	22
	S4.3. Tables of X-ray crystallography data collection and refinement parameters	25
S5.	Le Bail Refinements of the PXRD Data	26

S1. Main text supporting data

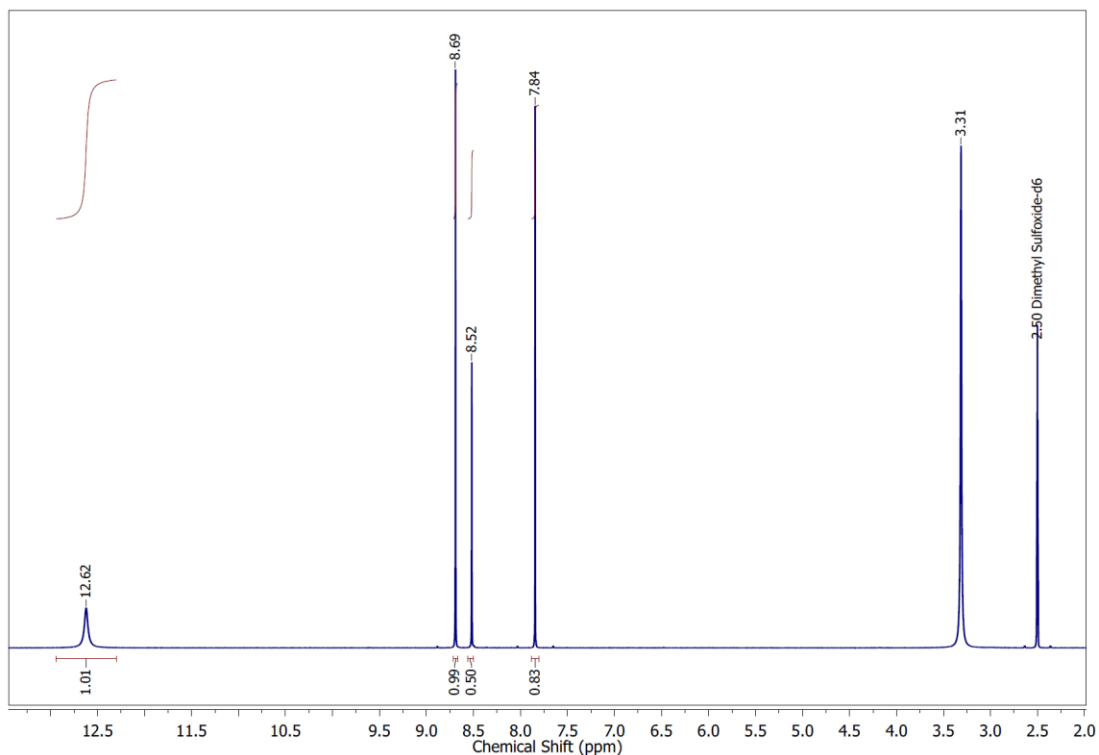


Figure S1. ^1H NMR spectrum of L1H_4 (500 MHz, DMSO-d_6): 12.62 (s, 4H, COOH), 8.69 (s, 4H, CH_2 pyrazole), 8.52 (s, 2H, N-CH-N), 7.84 (s, 4H, CH_2 pyrazole).

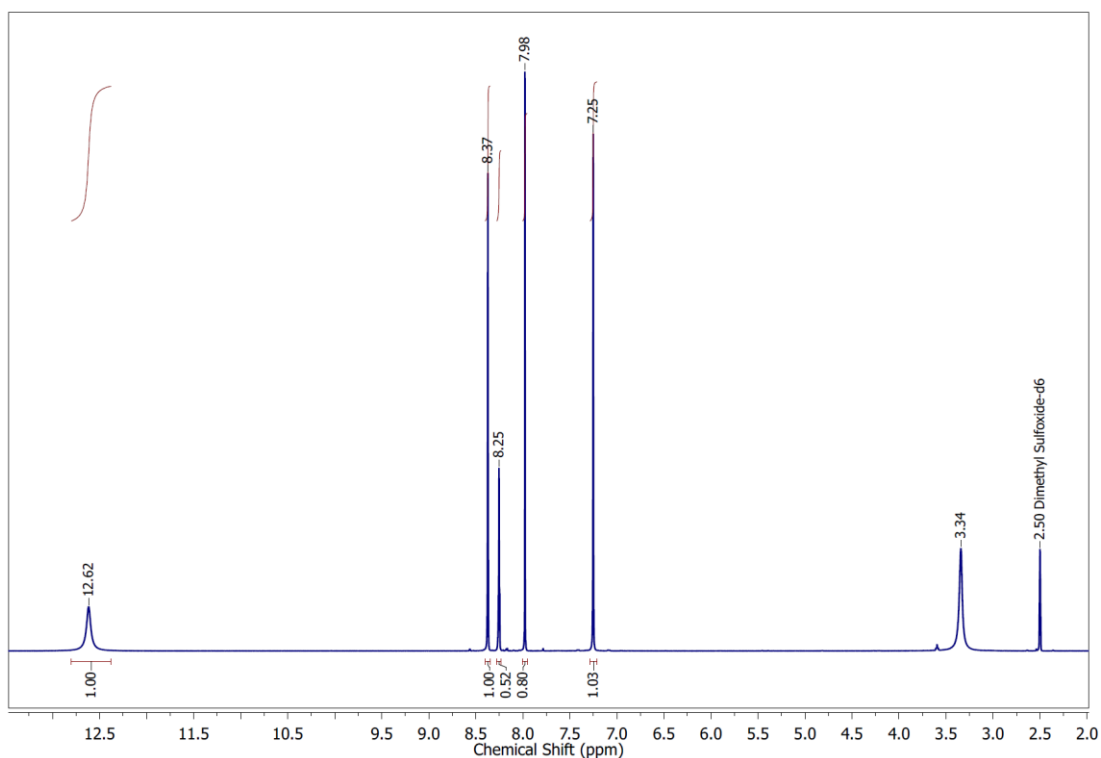


Figure S2. ^1H NMR spectrum of L2H_4 (500 MHz, DMSO-d_6): 12.62 (s, 4H, COOH), 8.37 (s, 4H, CH_2 pyrazole), 8.25 (s, 2H, N-CH-N), 7.98 (s, 4H, CH_2 pyrazole), 7.25 (s, 4H, CH phenyl).

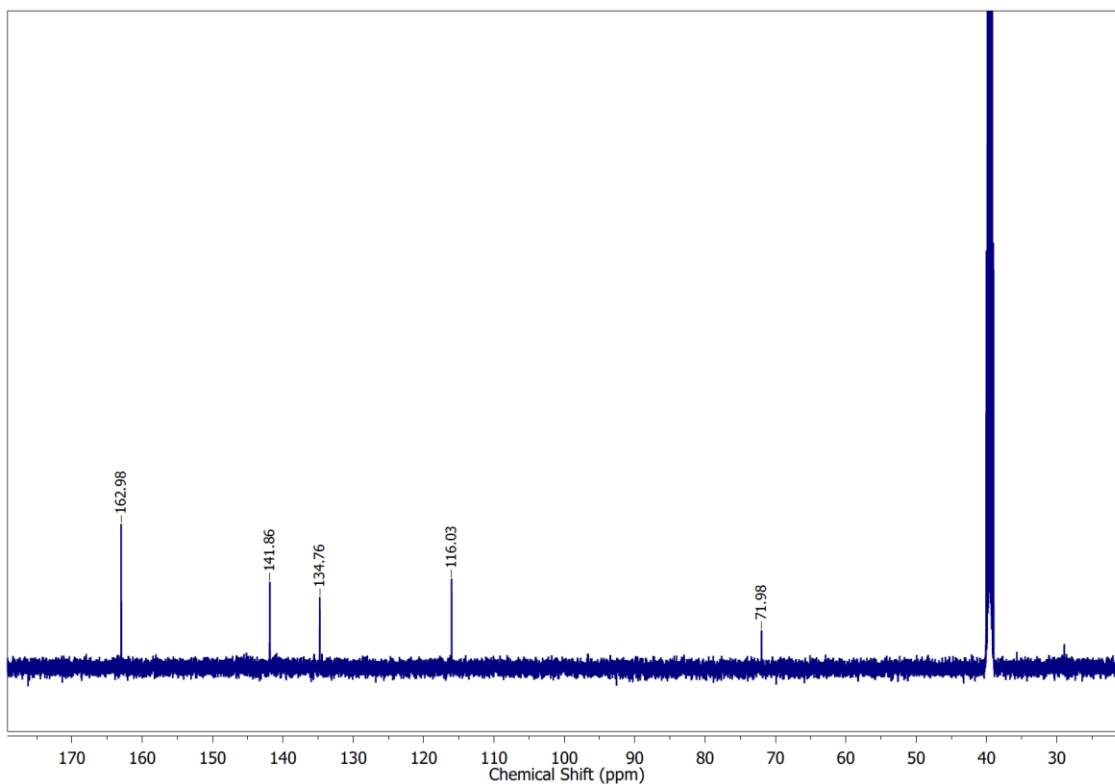


Figure S3. ^{13}C NMR spectrum of L1H_4 (500 MHz, DMSO-d_6): 162.98 (COOH), 141.86 (C pyr), 134.76 (C pyr), 116.03 (C pyr), 71.98 (C- sp^3).

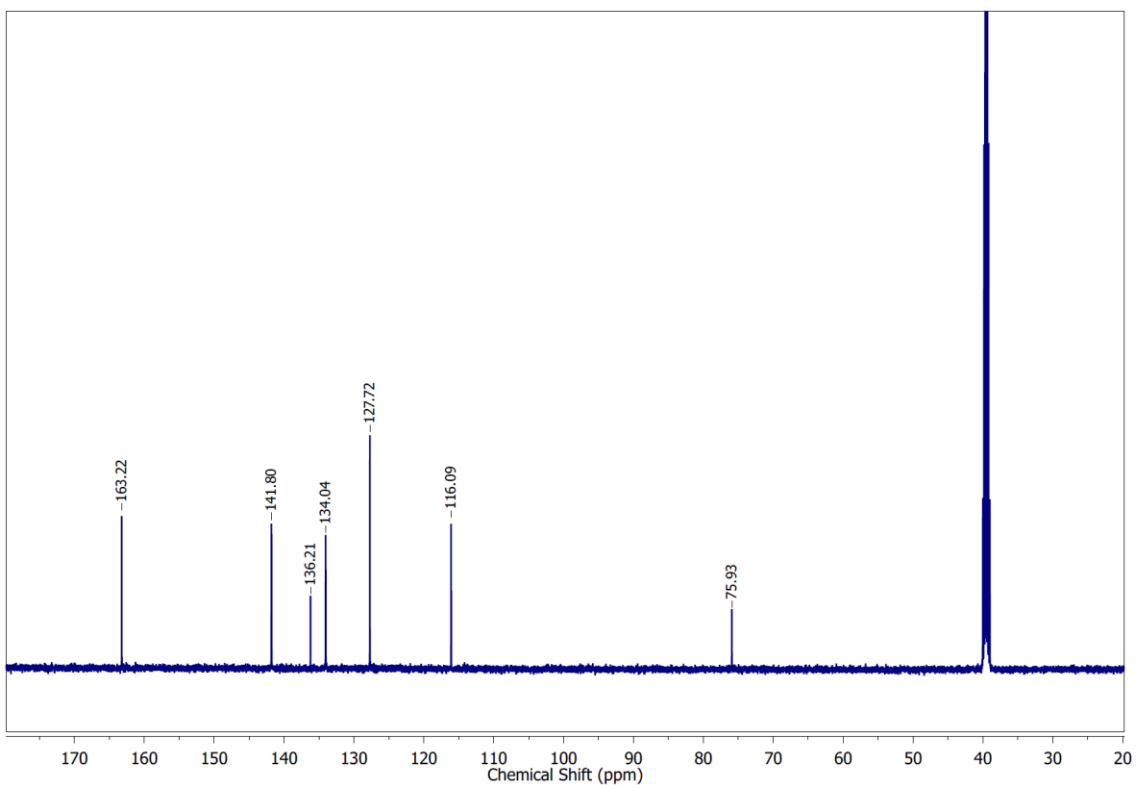


Figure S4. ^{13}C NMR spectrum of L2H_4 (500 MHz, DMSO-d_6): 163.22 (COOH), 141.80 (COOH), 136.21 (C pyr), 134.04 (C pyr), 127.72 (C phenyl), 116.09 (s, 4H, C pyr), 75.93 (C- sp^3).

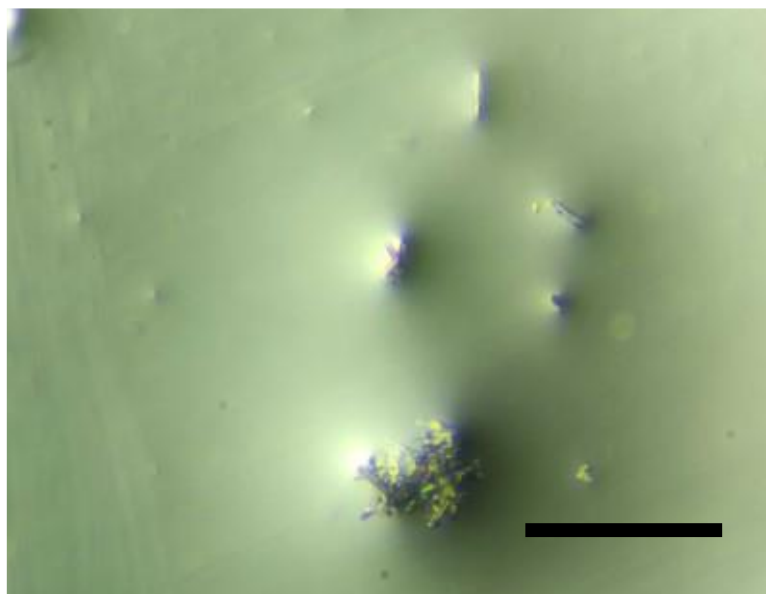


Figure S5. Photograph down the optical microscope of the UAM-10 crystals. Scale bar = 500 μm .

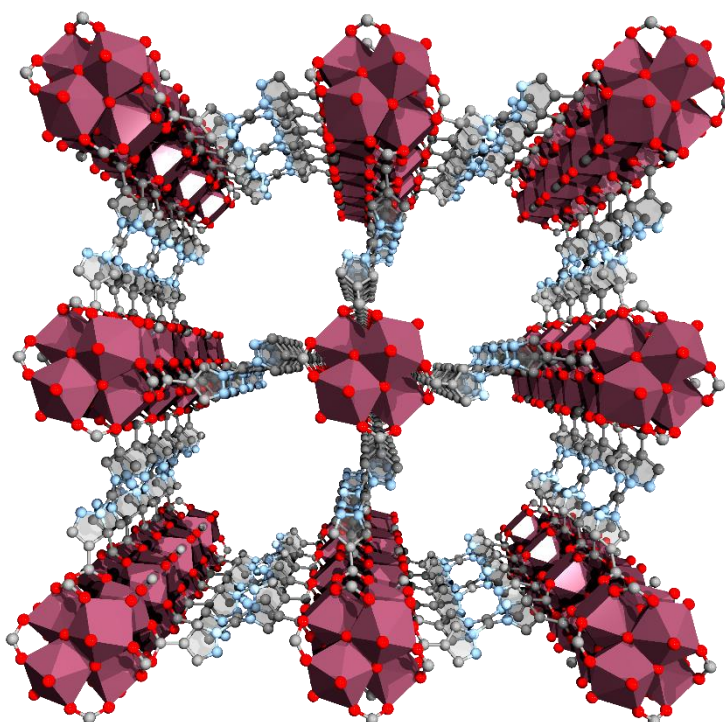


Figure S6. Representation of the structure of UAM-10 along the c axis (C, grey; N, light blue; O, red; Zr, dark red). Hydrogens have been omitted for clarity.

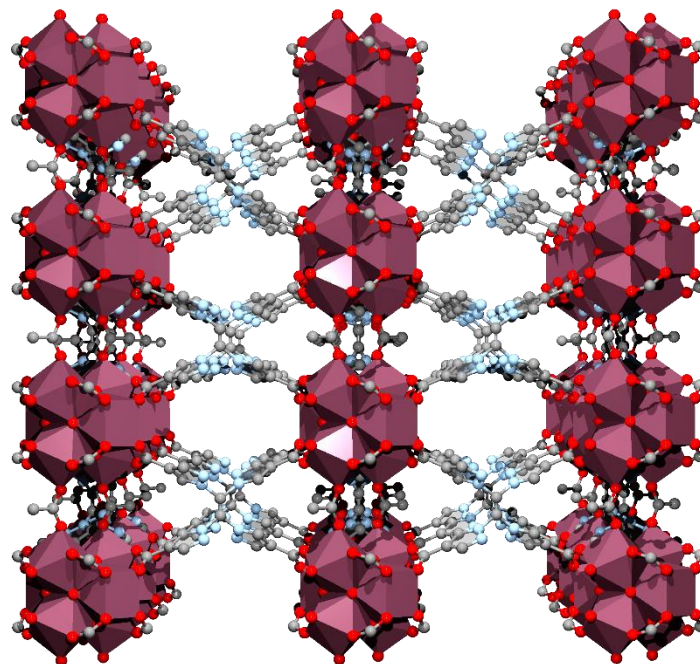


Figure S7. Representation of the structure of UAM-10 along the *a* axis (C, grey; N, light blue; O, red; Zr, dark red). Hydrogens have been omitted for clarity.

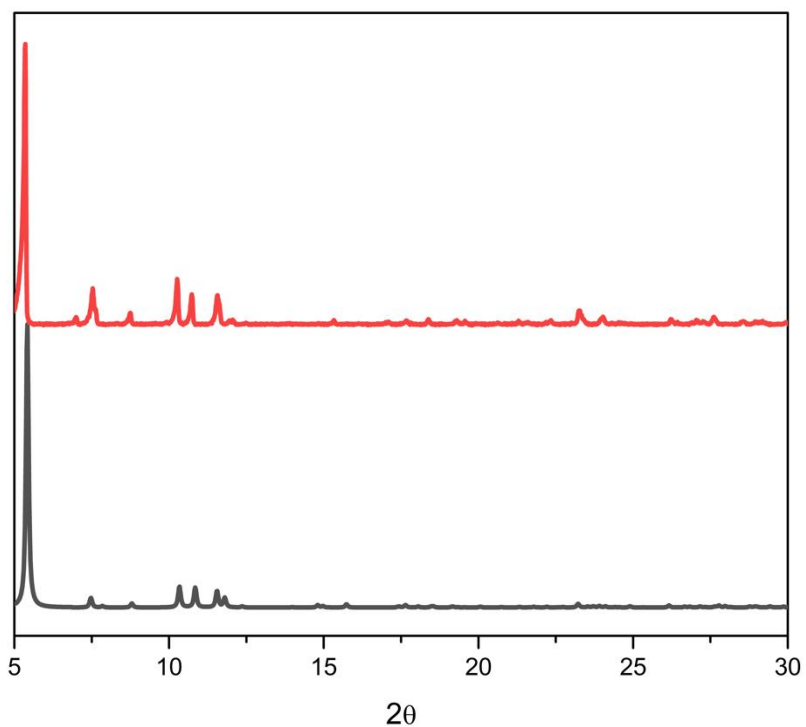


Figure S8. PXRD plots for **UAM-10 as made** (red) versus simulated **UAM-10** (black).

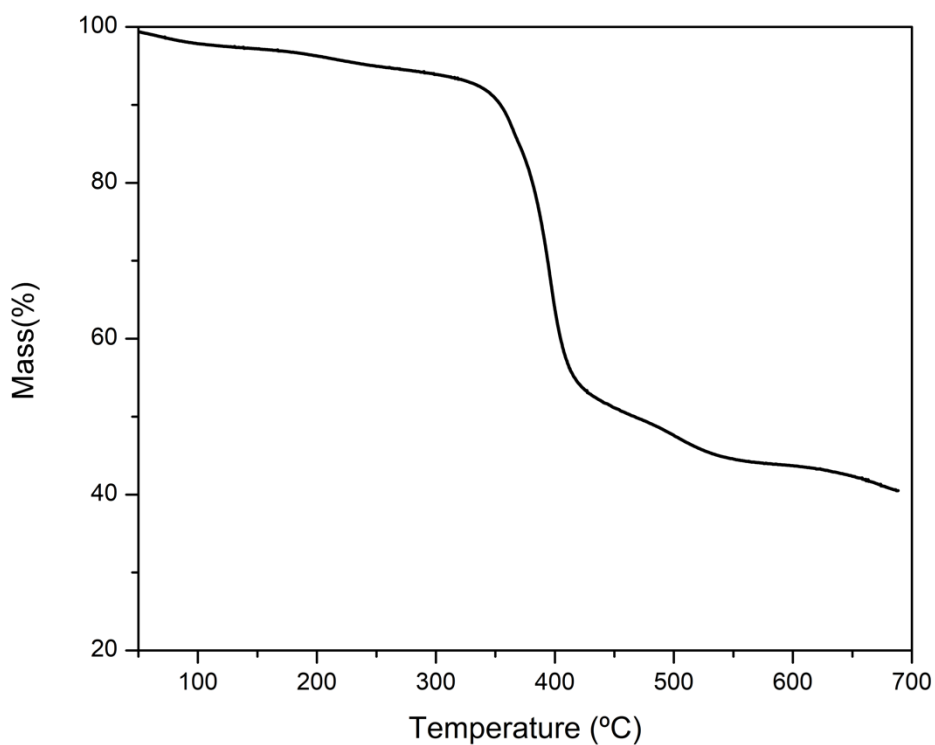


Figure S9. Thermogravimetric analysis plot for **UAM-10**. Analysis conditions: 50 °C – 700 °C at 5 °C/min, under an oxidising (air) atmosphere.

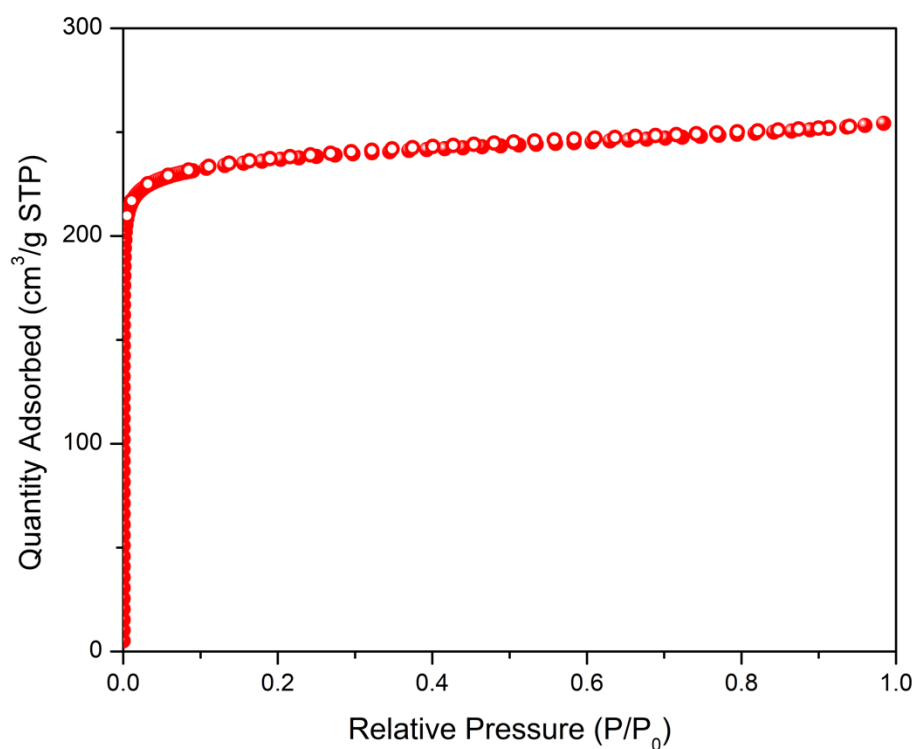


Figure S10. 77 K N_2 isotherm data of **UAM-10** after activation from acetone at 120 °C for 3 h. Filled circles represent adsorption; open circles represent desorption.

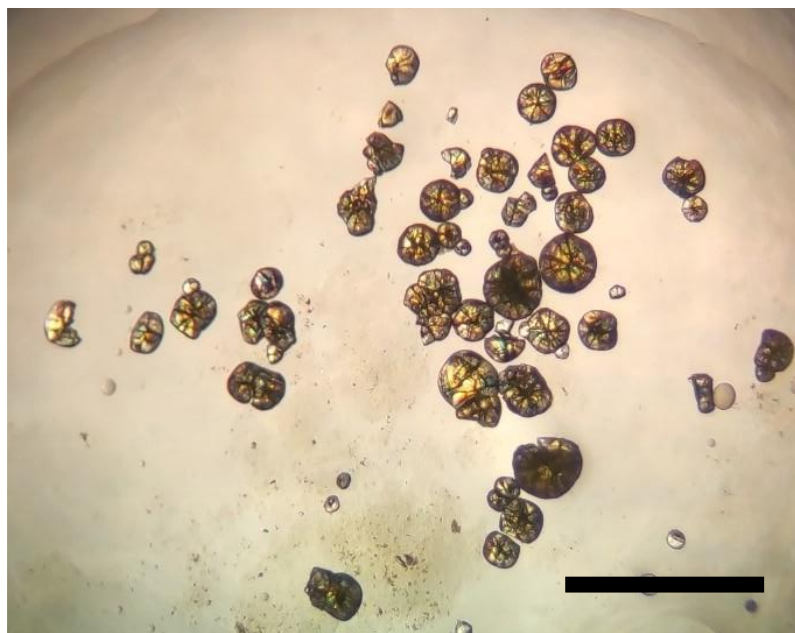


Figure S11. Optical image of UAM-11 crystals. Structure determination was conducted on crystals excised from the clumps. Scale bar = 500 μm .

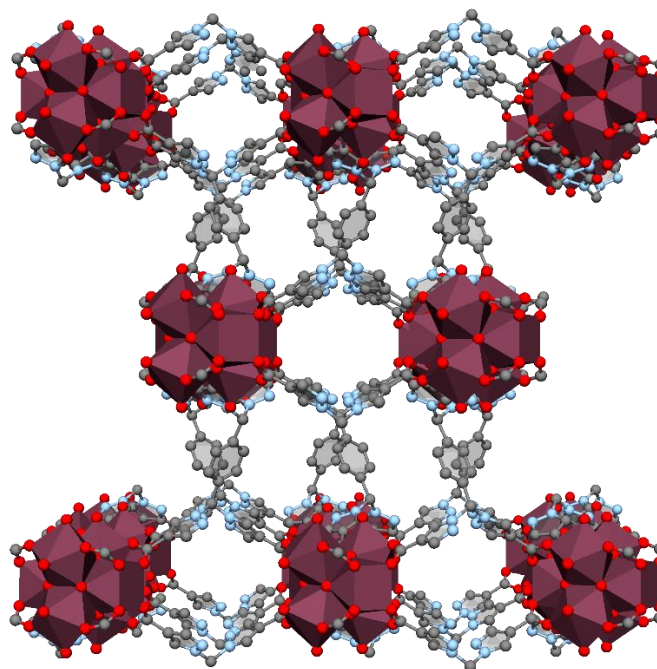


Figure S12. Representation of the structure of UAM-11 along the $(0,1,1)$ axis (C, grey; N, light blue; O, red; Cu, green; Zr, dark red; I, pink). Hydrogens have been omitted for clarity.

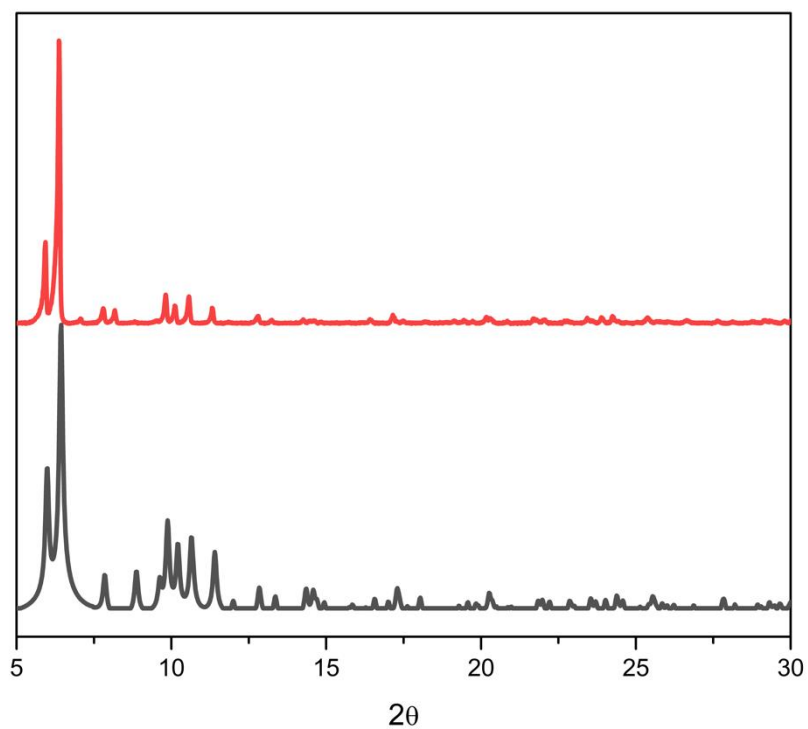


Figure S13. PXRD plots for **UAM-11 as made** (red) versus simulated **UAM-11** (black).

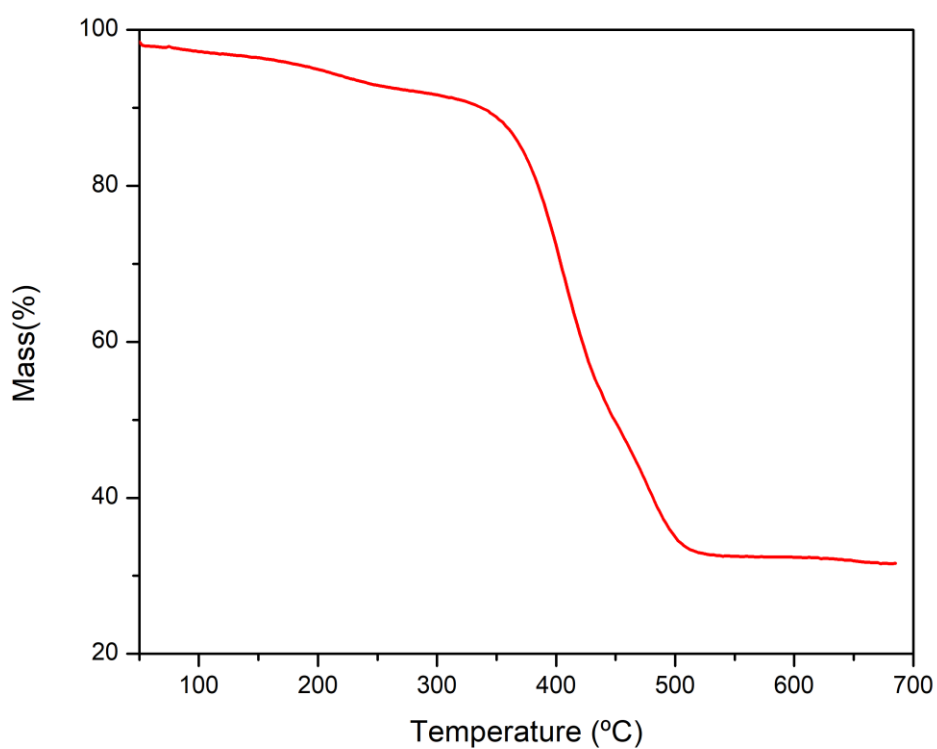


Figure S14. Thermogravimetric analysis plot of **UAM-11**. Analysis conditions: 50 °C – 700 °C at 5 °C/min, under an oxidising (air) atmosphere.

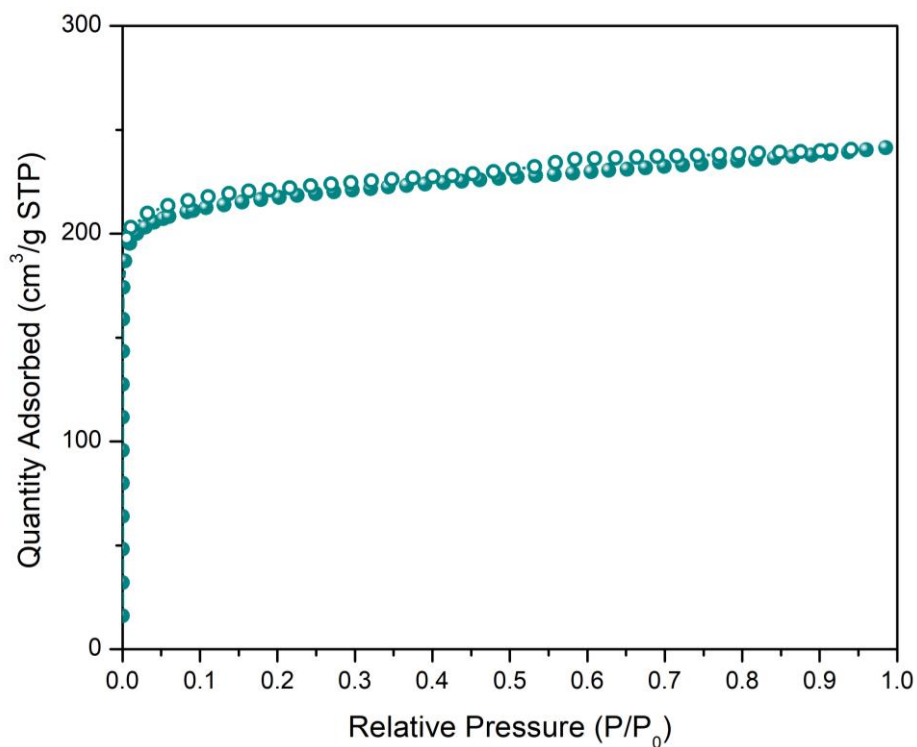


Figure S15. 77 K N_2 isotherm data of **UAM-11** after activation from acetone at 120 °C for 3 h. Filled circles represent adsorption; open circles represent desorption.

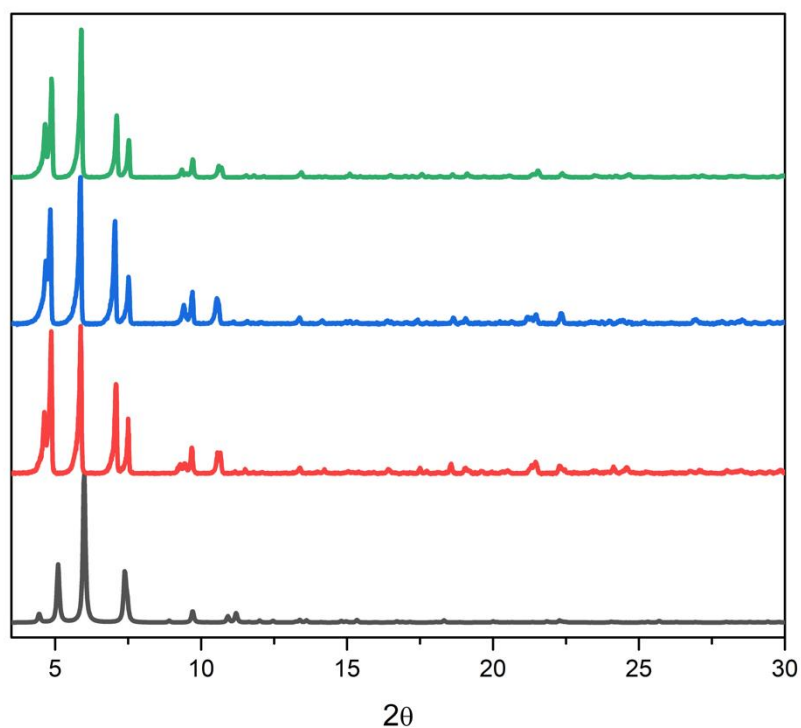


Figure S16. PXRD plots for **UAM-1000-BA as made** (red), **UAM-1000-AA as made** (blue) and **UAM-1000-TFA as made** (green) versus simulated **UAM-1000** (black). BA = benzoic acid, AA = acetic acid and TFA = trifluoroacetic acid.

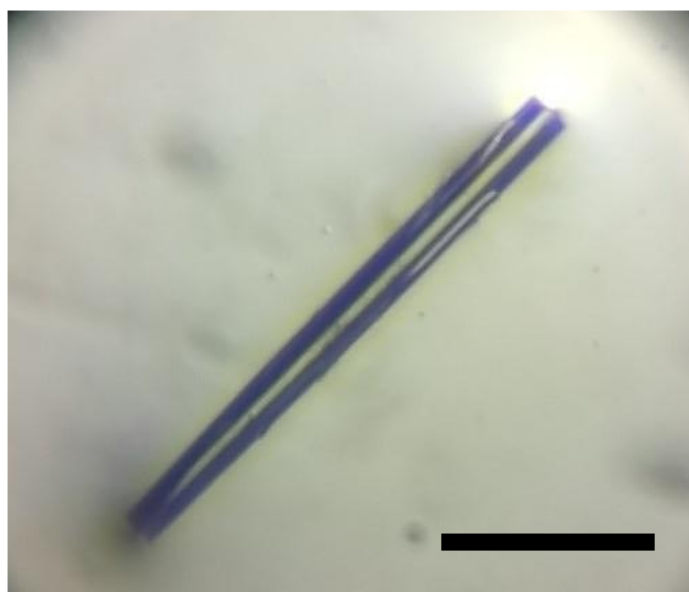


Figure S17. An image of a UAM-1002 crystal. Scale bar = 1 mm.

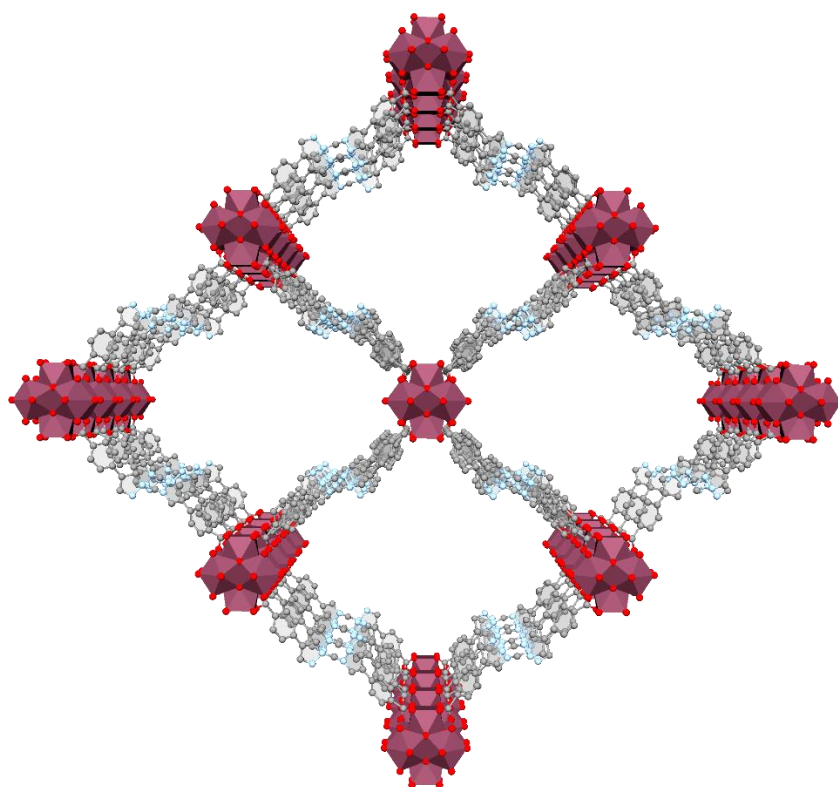


Figure S18. Representation of the structure of **UAM-1002** in the *ac* plane (C, grey; N, light blue; O, red; Cu, green; Zr, dark red; I, pink). Hydrogens have been omitted for clarity.

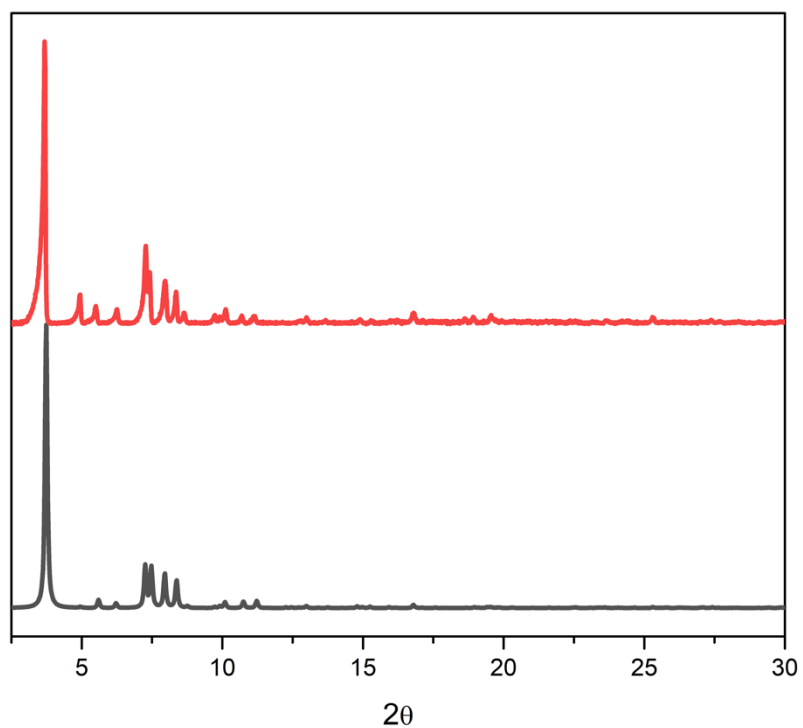


Figure S19. PXRD plots for **UAM-1002 as made** (red) versus simulated **UAM-1002** (black).

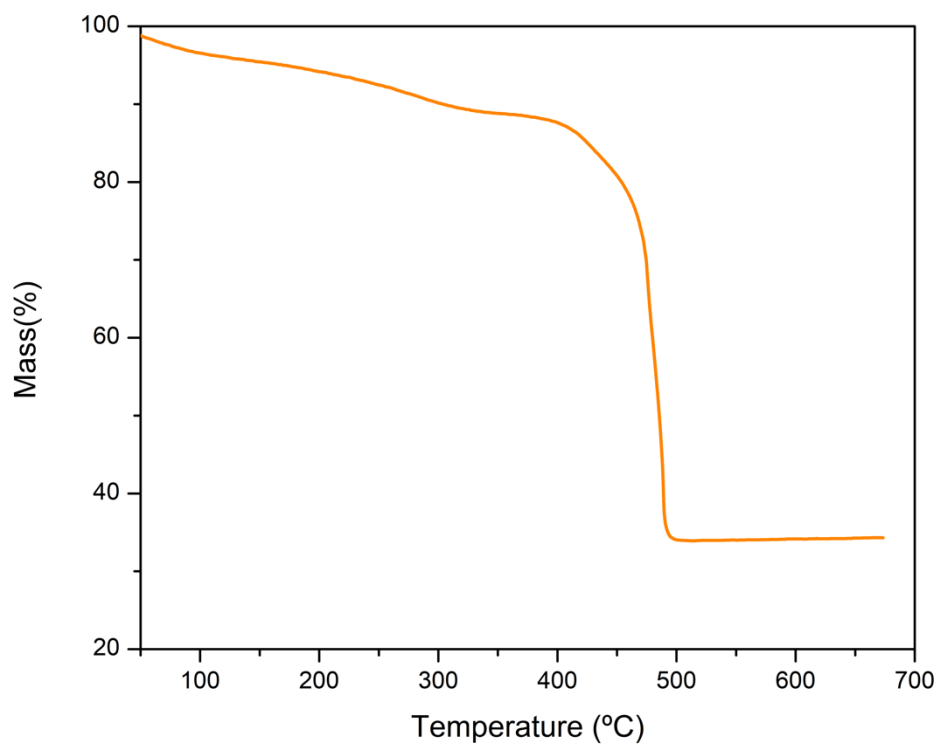


Figure S20. Thermogravimetric analysis spectrum of **UAM-1002** (black). Analysis conditions: 50 °C – 700 °C at 5 °C/min, under an oxidising (air) atmosphere.

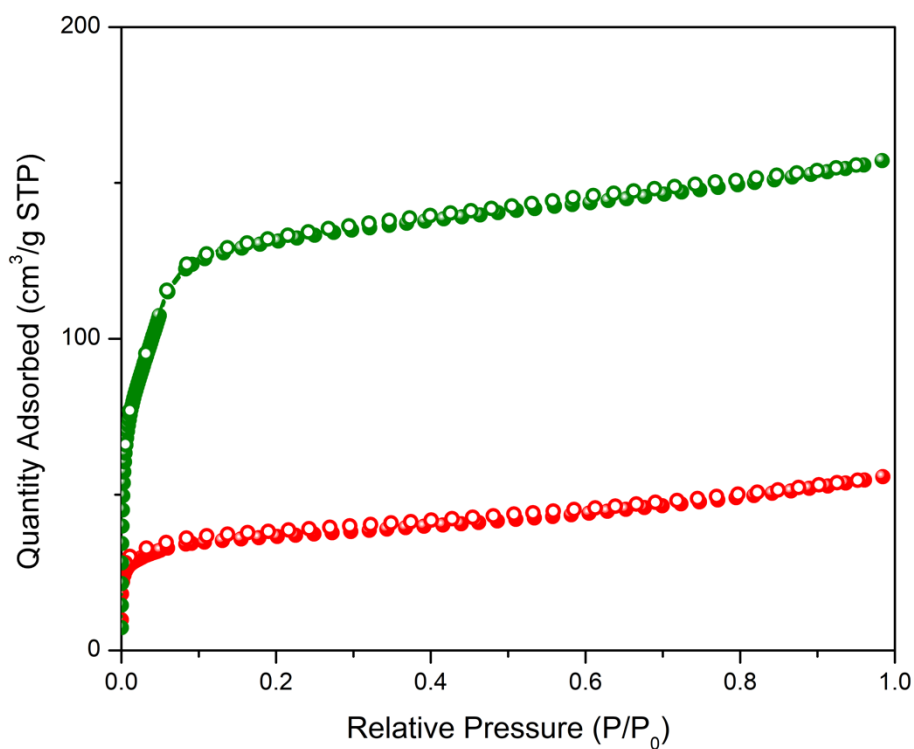


Figure S21. 77 K N_2 isotherm data of **UAM-1002** after activation from acetone at 120 °C for 3 h (red) and after activation with supercritical CO_2 (green). Filled circles represent adsorption, open circles represent desorption.

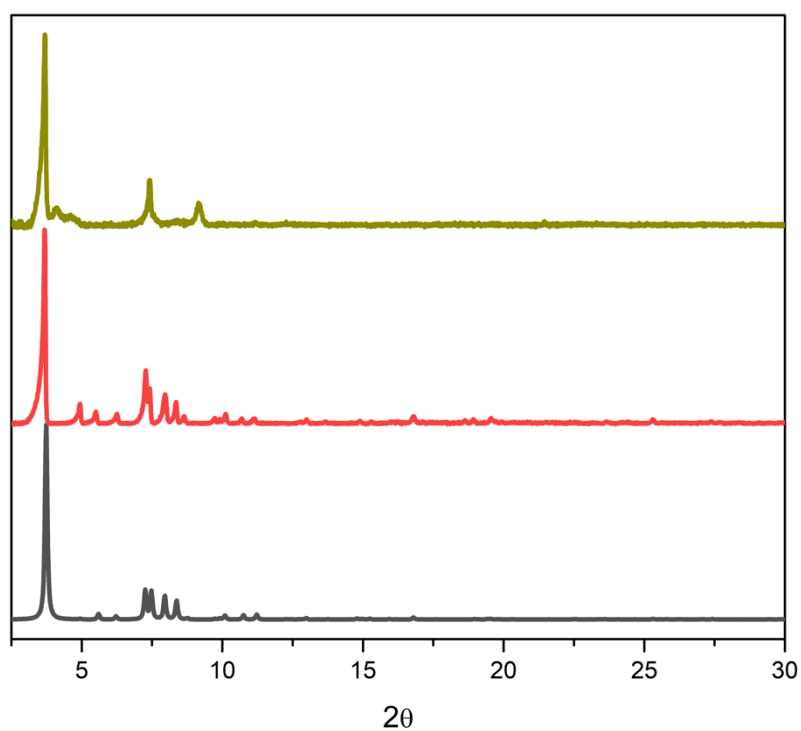


Figure S22. PXRD plots for **UAM-1002 as made** (red) and **UAM-1002-activated** (green) versus simulated **UAM-1002** (black). **UAM-1002** was activated using supercritical CO_2 .

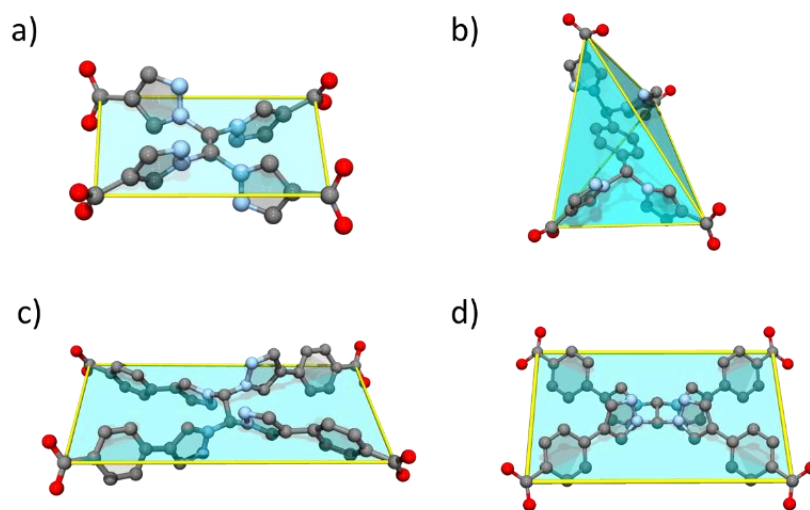


Figure S23. Representations of the organic linkers in their respective MOF structures. a) L1 in UAM-10, b) L2 in UAM-11, c) L3 in UAM-1002 and d) L3 in UAM-1000.

Table S1. Summary of the properties computed for the hypothetical frameworks formed with L1, L2 and TCPE. The blue text highlights MOFs reported experimentally in this work.

Ligand	Topology	DFT energy [eV/atom]	Density (g/ cm ³)	Accessible pore volume (cm ³ /g)	Accessible surface area (m ² /g)
L1	csq	-255.275	0.853	0.516	1444
L1	flu	-255.263	1.075	0.260	1544
L1	scu	-255.146	1.927	0.018	0
L1	sqc	-255.270	1.304	0.122	880
L2	csq	-233.897	0.600	0.945	2220
L2	flu	-233.883	0.936	0.349	1996
L2	scu	-233.900	1.267	0.172	1190
L2	sqc	-233.718	1.358	0.092	546
TCPE	csq	-194.683	0.393	1.691	3626
TCPE	flu	-194.681	0.513	1.085	3683
TCPE	scu	-194.678	0.473	1.236	3648
TCPE	sqc	-194.679	1.298	0.126	905

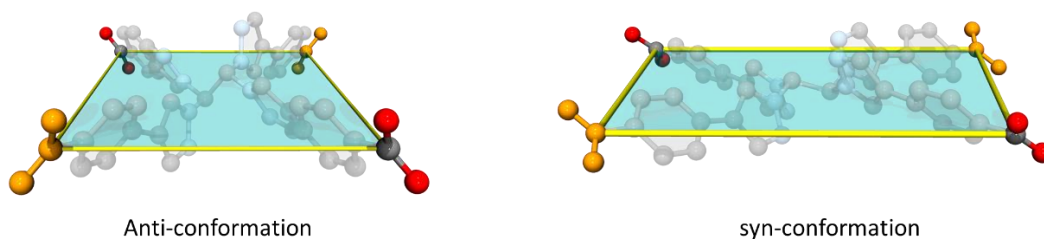


Figure S24. Representations of TCPE in UAM-1002 (left) with its anti-conformation of the bispyrazole groups and UAM-1000 (right) in its syn conformation. The carboxylates that change orientation are highlighted in orange.

Table S2. Relative UFF energies (kJ/mol per atom) for L1 and TPCE for different ligand conformations.

ligand	topology	syn-syn	anti-anti
1	csq	0.821	1.459
1	flu	3.489	1.875
1	scu	0.000	1.100
1	sqc	2.544	2.759
TCPE	csq	0.000	0.571
TCPE	flu	-	0.688
TCPE	scu	0.219	0.634
TCPE	sqc	0.090	2.359

Table S3. Energy-dispersive X-ray (EDX) data for Pd and Cl before and after metalation of **UAM-10**, **UAM11** and **UAM1002**. The % occupancy in the bis(pyrazolyl)methane coordinating sites was determined by measuring Zr:Pd and Pd:Cl ratios.

Sample	Pd (% occupancy) ^{a,b}	Cl (% occupancy) ^{a,b}
UAM-10 · PdCl ₂	23.2 ± 10	59.4 ± 14
UAM-11 · PdCl ₂	10.0 ± 9	22.3 ± 14
UAM-1002 · PdCl ₂	98.5 ± 3	200 ± 3

^a Average atomic% obtained from three areas of three different crystals.

^b Relative to full occupancy of the bis(pyrazolyl)methane sites in the corresponding MOF (Zr:M = 3:2).

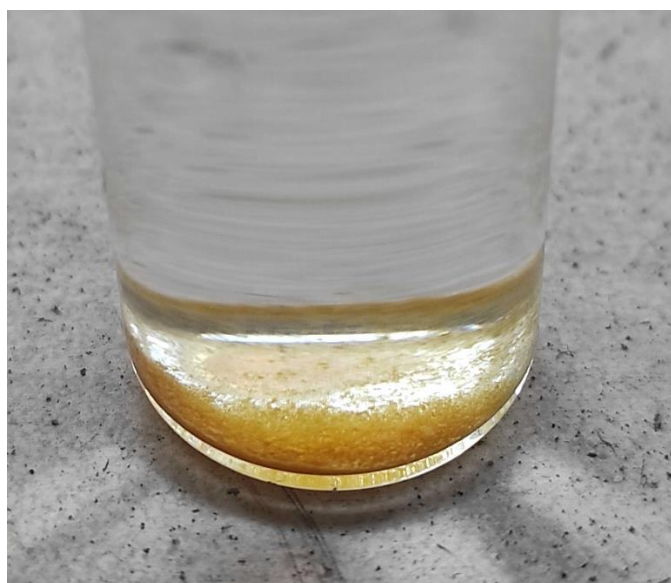


Figure S25. Image of bulk **UAM-1002**[PdCl₂] showing the orange colouration of the crystals.

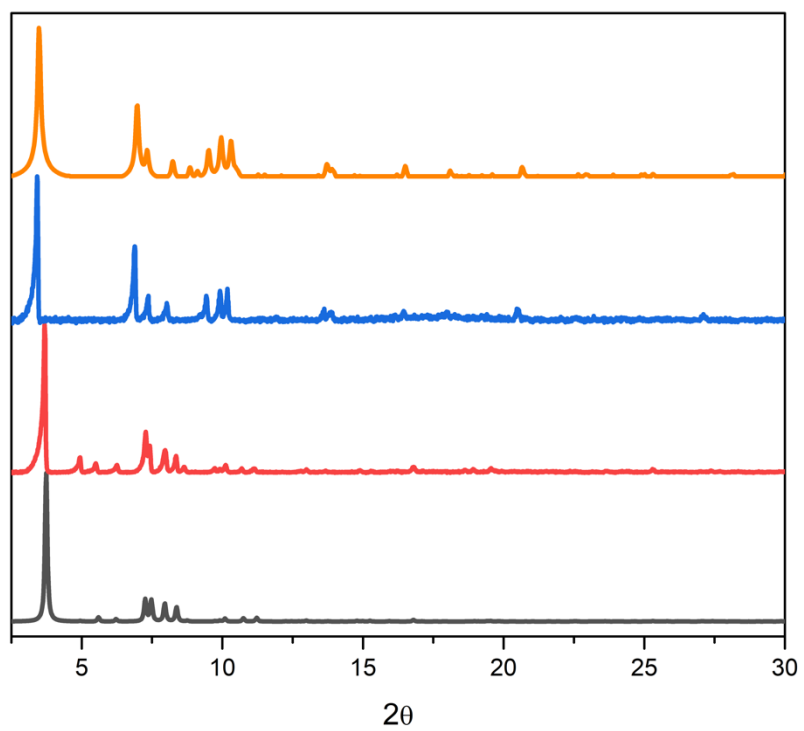


Figure S26. PXRD plots for **UAM-1002 as made** (red) versus simulated **UAM-1002** (black) and **UAM-1002[PdCl₂] as made** (blue) versus simulated **UAM-1002[PdCl₂]** (orange).

S2. Fourier Transform Infrared Spectroscopy (FTIR) spectra

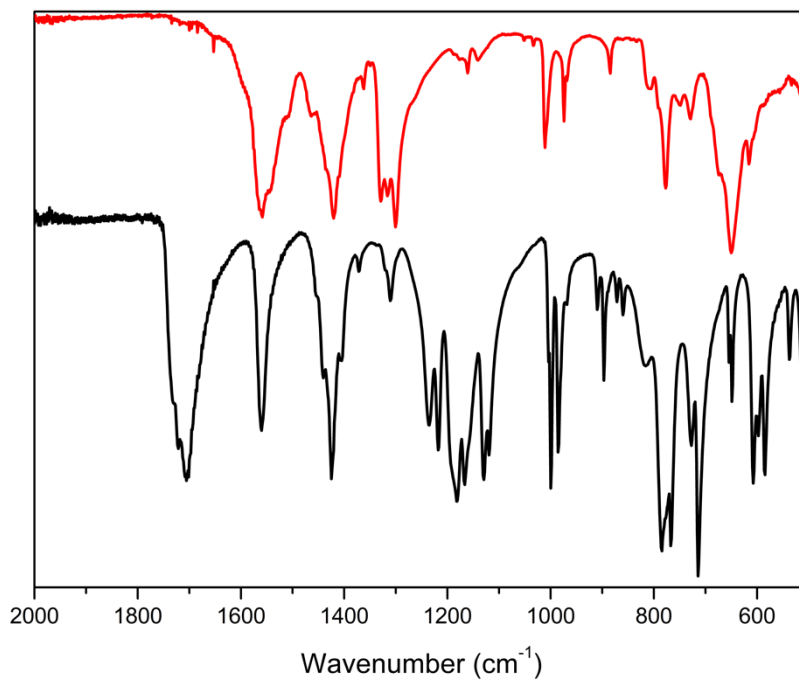


Figure S27. FTIR spectra of **L1H₄** (black) and **UAM-10** as made (red).

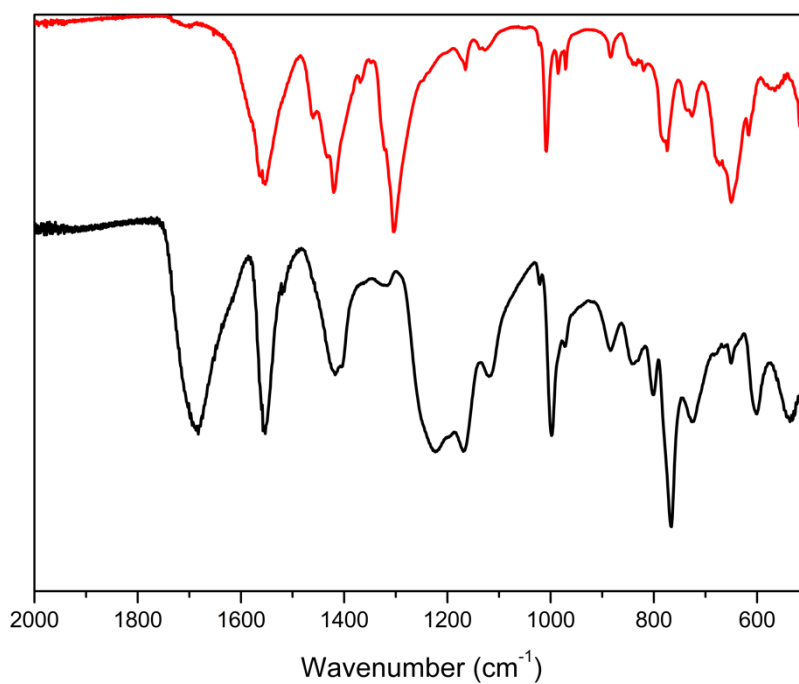


Figure S28. FTIR spectra of **L2H₄** (black) and **UAM-11** as made (red).

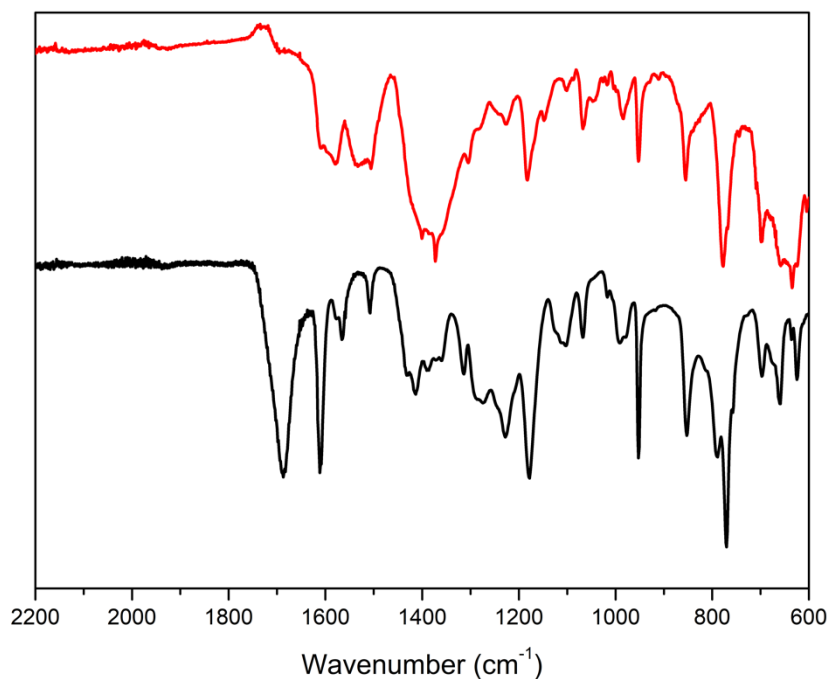


Figure S29. FTIR spectra of **TCPE** (black) and **UAM-1002** as made (red).

S3. Adsorption experiments

Table S4. Experimental and simulated BET surface areas based on the crystal structures for UAM-10, UAM-11, UAM-1000 and UAM-1002 ($\text{m}^2 \text{g}^{-1}$).

Sample	Experimental	Calculated
UAM-10	864	1300
UAM-11	844	2400
UAM-1000	391	3100
UAM-1002	567	3400

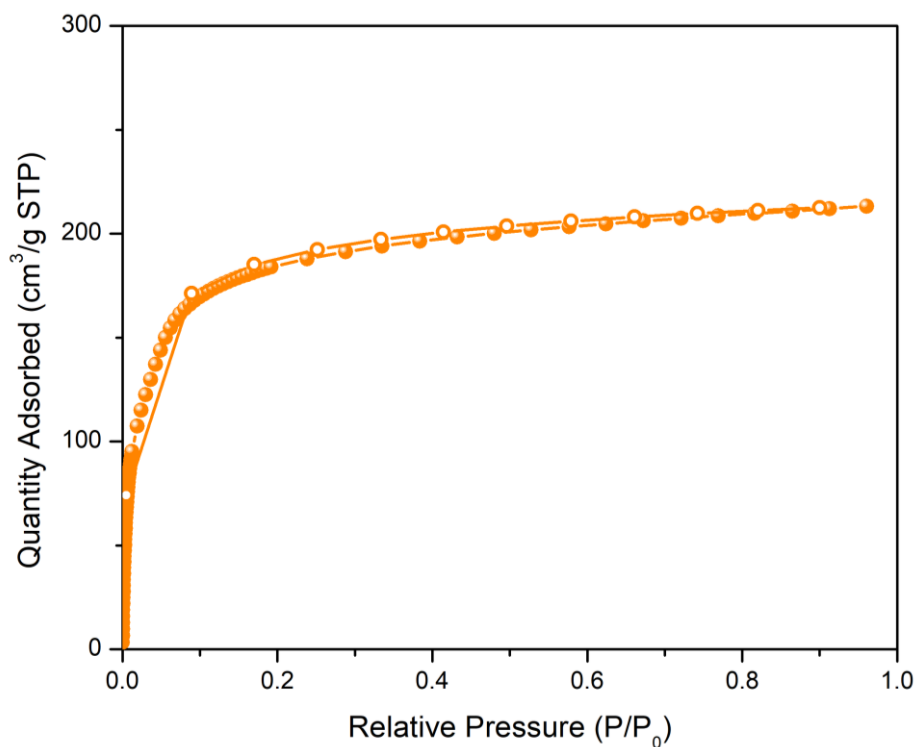


Figure S30. 195 K CO₂ isotherm of **UAM-10** after activation from acetone at 120 °C for 3 h. Filled circles represent adsorption; open circles represent desorption.

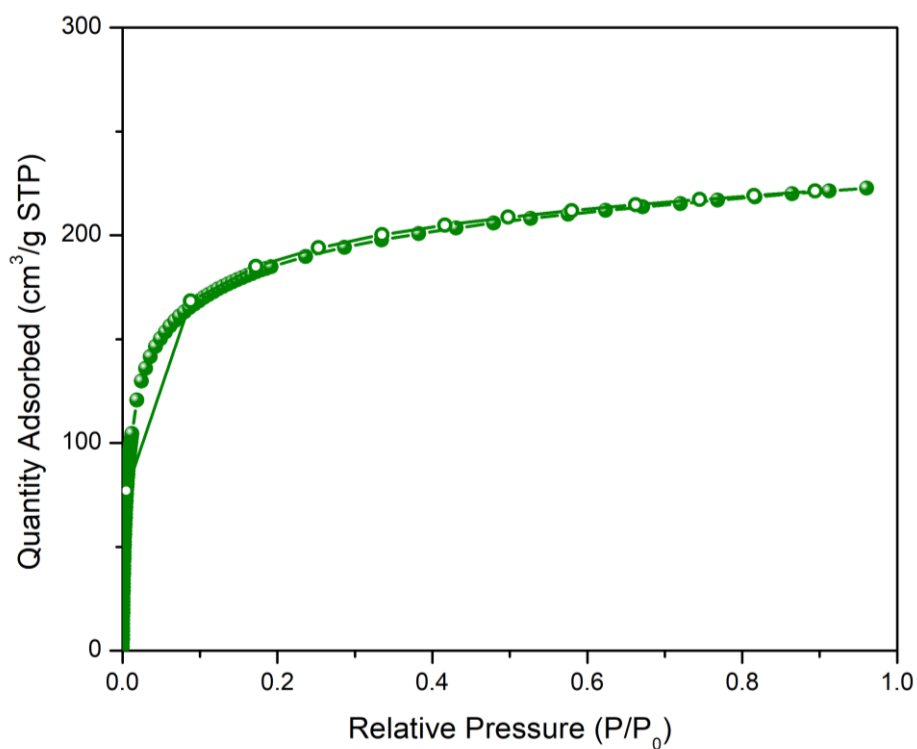


Figure S31. 195 K CO₂ isotherm of **UAM-11** after activation from acetone at 120 °C for 3 h. Filled circles represent adsorption; open circles represent desorption.

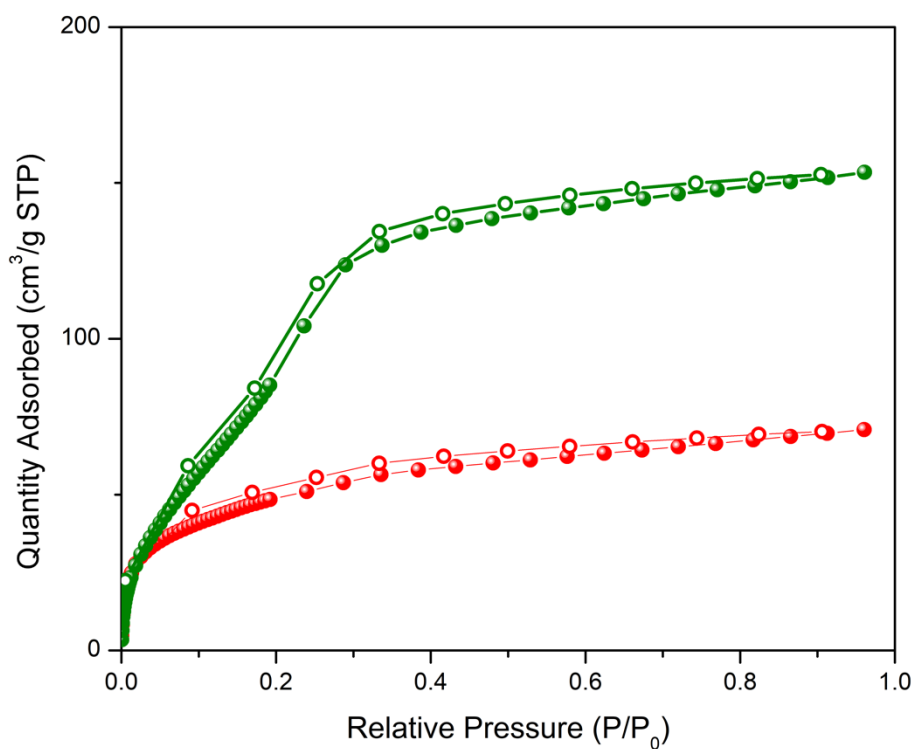


Figure S32. 195 K CO₂ isotherm of UAM-1002 after activation from acetone at 120 °C for 3 h (red) and after activation under supercritical CO₂ (green). Filled circles represent adsorption; open circles represent desorption.

S4. Single crystal X-ray crystallography

S4.1. Specific Data and Refinement Details

UAM-10. The pyrazole rings were modelled by adding them as a fragment. The atoms corresponding to the DMF molecule in the pore were left isotropic as they are too disordered to allow anisotropic refinement.

UAM-11. No special refinement details.

UAM-1002. The phenyl and pyrazole rings were modelled with AFIX restraints due to the crystallographic disorder.

UAM-1002[PdCl₂]. Some of the atoms of the pyrazole rings had to be modelled with EADP restraints due to the proximity of the atoms arising from crystallographic disorder of the pyrazole rings.

S4.2. Thermal ellipsoid plots for all structures at the 50% probability level

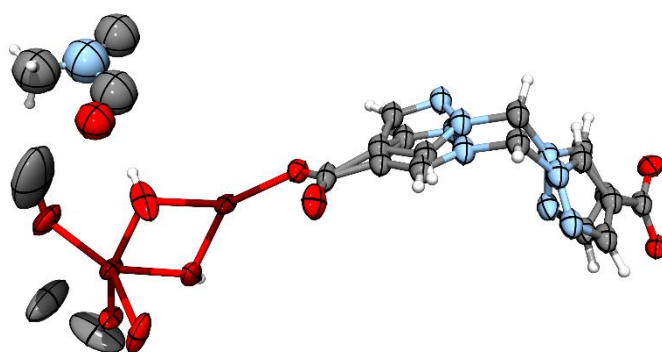


Figure S33. Asymmetric unit of **UAM-10**, with all non-hydrogen atoms represented by ellipsoids at the 50% probability level (C, grey; H, white; N, light blue; O, red; Zr, dark red).

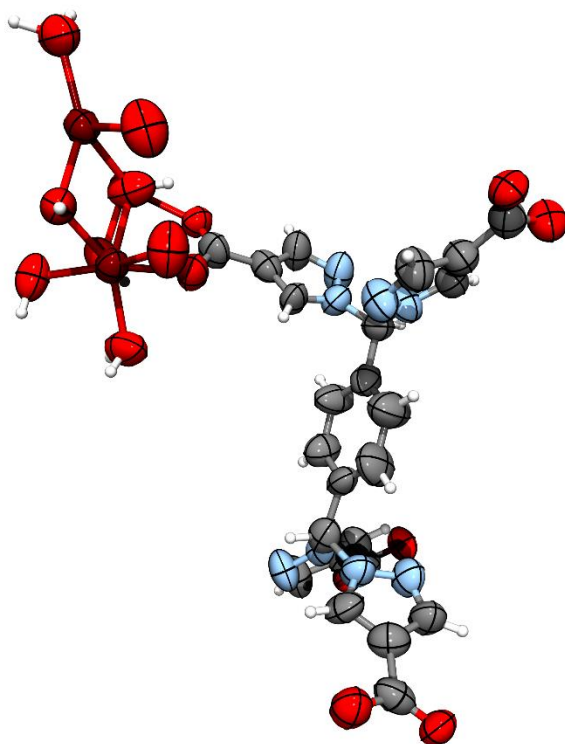


Figure S34. Asymmetric unit of **UAM-11**, with all non-hydrogen atoms represented by ellipsoids at the 50% probability level (C, grey; H, white; N, light blue; O, red; Zr, dark red).

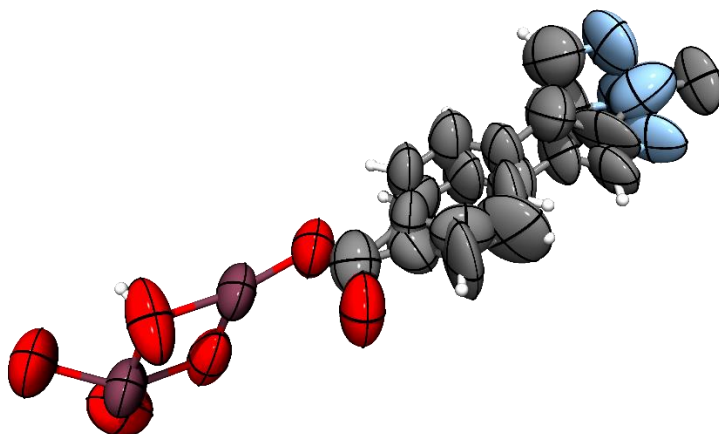


Figure S35. Asymmetric unit of **UAM-1002**, with all non-hydrogen atoms represented by ellipsoids at the 50% probability level (C, grey; H, white; N, light blue; O, red; Zr, dark red).

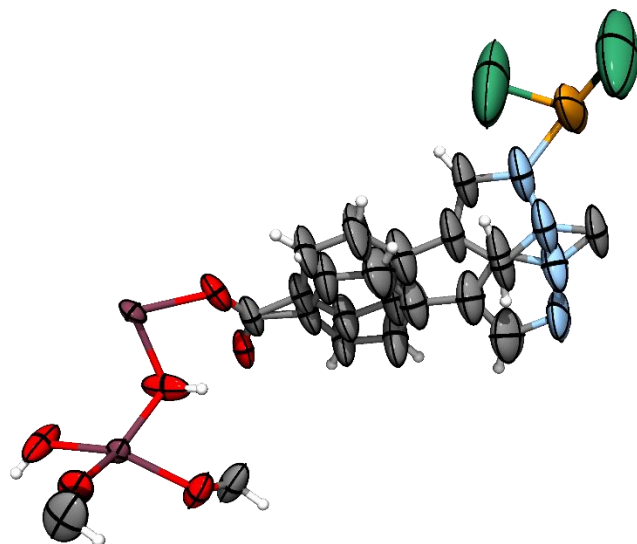


Figure S36. Asymmetric unit of **UAM-1002[PdCl₂]**, with all non-hydrogen atoms represented by ellipsoids at the 50% probability level (C, grey; H, white; N, light blue; O, red; Zr, dark red; Pd, orange; Cl, chlorine).

S4.3. Tables of X-ray crystallography data collection and refinement parameters

Table S5. Crystallographic data collection and refinement parameters for **UAM-10**, **UAM-11**, **UAM-1002** and **UAM-1002[PdCl₂]**.

Sample	UAM-10	UAM-11	UAM-1002	UAM-1002-PdCl ₂
Crystallographic Parameter				
Formula	C ₁₂ H ₈ N _{4.5} O _{8.5} Zr _{1.5}	C ₁₂ H ₁₁ N ₄ O ₈ Zr _{1.5}	C _{10.5} H ₇ N ₂ O ₄ Zr _{0.75}	C ₁₁ H _{7.5} ClN ₂ O ₄ Pd _{0.5} Zr _{0.75}
FW	488.06	476.08	293.6	388.75
T, K	100(2)	100(2)	100(2)	100(2)
Wavelength, Å	monoclinic	orthorhombic	orthorhombic	orthorhombic
Crystal system, space group	<i>C2/m</i>	<i>Cmce</i>	<i>Cmmm</i>	<i>Cmmm</i>
Z	22.511(5)	29.301(7)	33.273(7)	33.4742(5)
a, Å	23.641(5)	22.313(8)	35.780(7)	38.7659(6)
b, Å	10.046(2)	21.132(4)	12.220(2)	9.98330(10)
c, Å	90	90	90	90
α°	90.01(3)	90	90	90
β, °	90	90	90	90
γ°	5346.3(18)	13816(7)	14548(5)	12954.9(3)
V, Å ³	8	16	16	16
d _{calc} , g/cm ³	1.213	0.916	0.536	0.797
Absorption coefficient, mm ⁻¹	0.63	0.485	0.236	5.14
F(000)	1916	3760	2336	3032
Crystal size, mm ³	0.104 × 0.063 × 0.02	0.04 × 0.035 × 0.028	0.197 × 0.031 × 0.027	0.174 × 0.042 × 0.03
Radiation	Synchrotron (λ = 0.71073)	Synchrotron (λ = 0.71073)	Synchrotron (λ = 0.71073)	Cu Kα (λ = 1.54184)
2θ range for data collection	2.498 to 57.294	2.78 to 57.368	1.672 to 57.364	5.28 to 152.882
Index range	-30 ≤ h ≤ 29, -29 ≤ k ≤ 29, -13 ≤ l ≤ 13	-38 ≤ h ≤ 39, -29 ≤ k ≤ 29, -25 ≤ l ≤ 25	-43 ≤ h ≤ 43, -47 ≤ k ≤ 46, -16 ≤ l ≤ 16	-40 ≤ h ≤ 38, -48 ≤ k ≤ 39, -12 ≤ l ≤ 9
Reflections collected	33666	84271	86300	34370
Independent reflections	5477 [R _{int} = 0.0732, R _{sigma} = 0.0435]	7571 [R _{int} = 0.2390, R _{sigma} = 0.1079]	8298 [R _{int} = 0.1189, R _{sigma} = 0.0614]	6887 [R _{int} = 0.0392, R _{sigma} = 0.0307]
Data/restraints/parameters	5477/87/220	7571/0/235	8298/0/236	6887/0/222
GOF on F ²	1.06	0.878	0.936	1.134
Largest diff. peak and hole, eÅ ⁻³	1.33/-0.74	0.52/-0.89	0.44/-1.00	0.86/-1.28
R ₁ , [I > 2σ(I)]	0.0560	0.0716	0.1144	0.0488
wR ₂ , all data	0.1705	0.2304	0.3759	0.1507
CCDC Number	2288076	2288077	2288079	2288078

S5. Le Bail Refinements of the PXRD Data

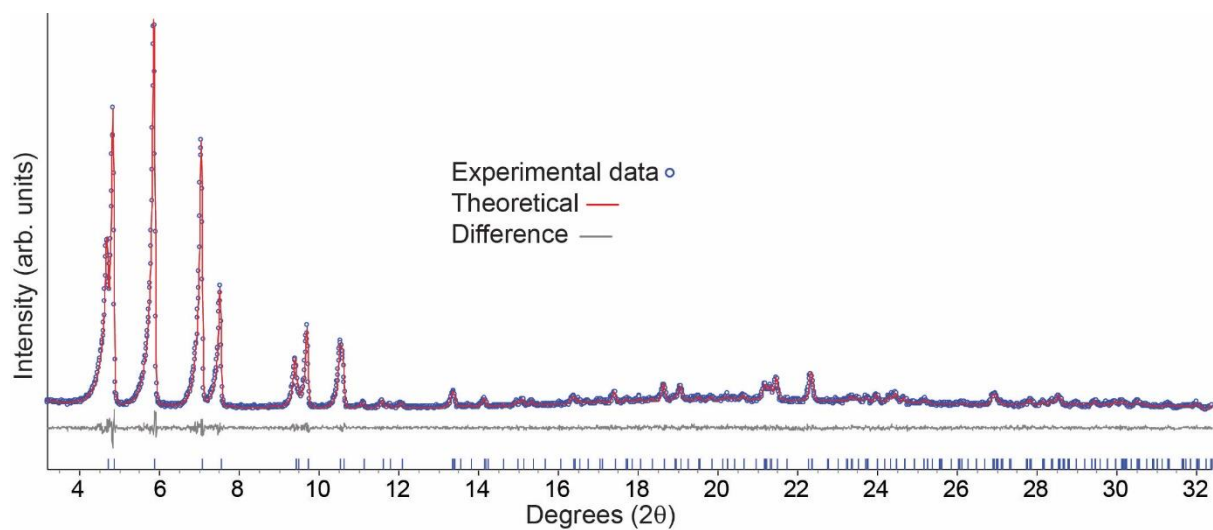


Figure S37. Le Bail refinement of the Powder X-ray diffraction pattern of **UAM-1000**. Refinement parameters: $R_p = 5.64$, $R_{wp} = 7.70$, $GoF = 1.15$. Cell parameters $I4_1/amd$, $a = 18.7$; $c = 75.0$ Å. For comparison, the cell parameters of the single crystal X-ray structure: $I4_1/amd = 17.9$; $c = 78.8$ Å.

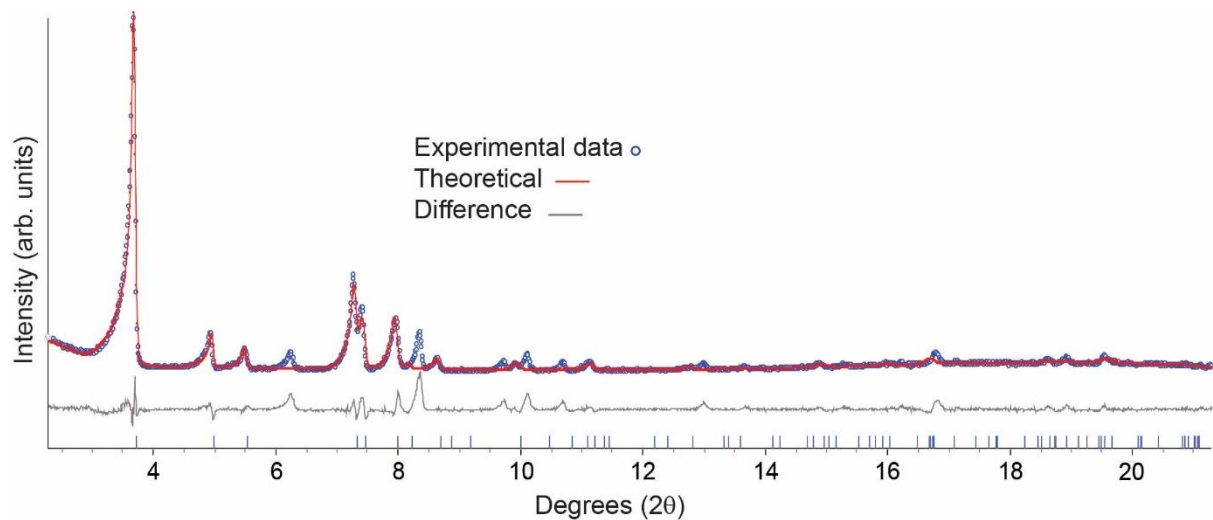


Figure S38. Le Bail refinement of the Powder X-ray diffraction pattern of **UAM-1002**. Refinement parameters: $R_p = 10.07$, $R_{wp} = 16.62$, $GoF = 3.40$. Cell parameters $Cmmm$, $a = 31.8$; $b = 35.3$; $c = 12.1$ Å. For comparison, the cell parameters of the single crystal X-ray structure: $Cmmm = a = 33.3$; $b = 35.8$; $c = 12.2$ Å.

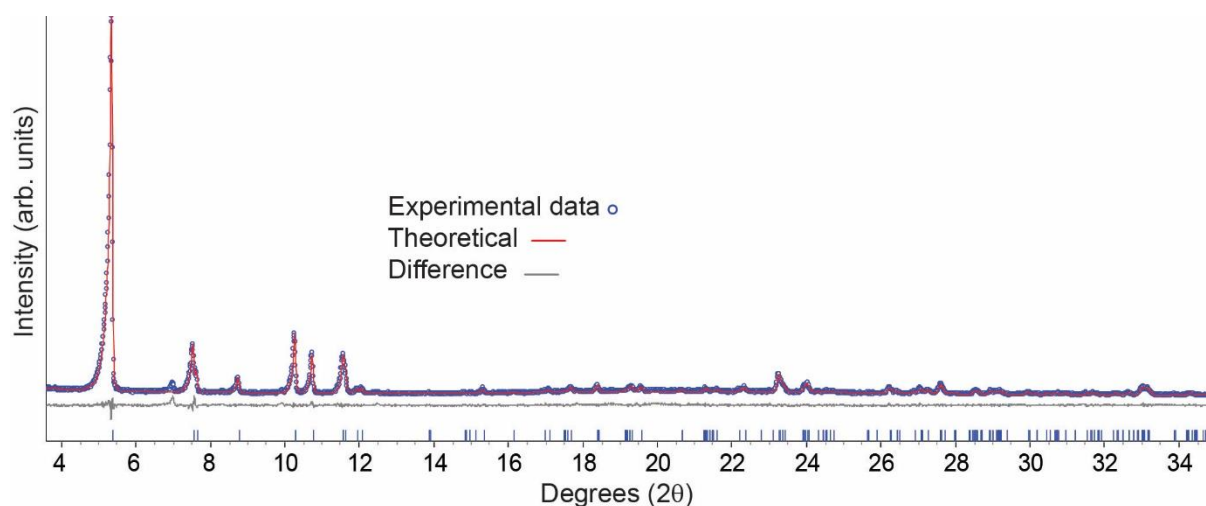


Figure 39. Le Bail refinement of the Powder X-ray diffraction pattern of **UAM-10**. Refinement parameters: $R_p = 6.53$, $R_{wp} = 9.50$, $GoF = 1.34$. Cell parameters $C2/m$, $a = 23.4$; $b = 23.1$; $c = 10.0 \text{ \AA}$; $\beta = 90.1^\circ$. For comparison, the cell parameters of the single crystal X-ray structure: $C2/m$, $a = 22.5$; $b = 23.6$; $c = 10.0 \text{ \AA}$; $\beta = 90.0^\circ$.

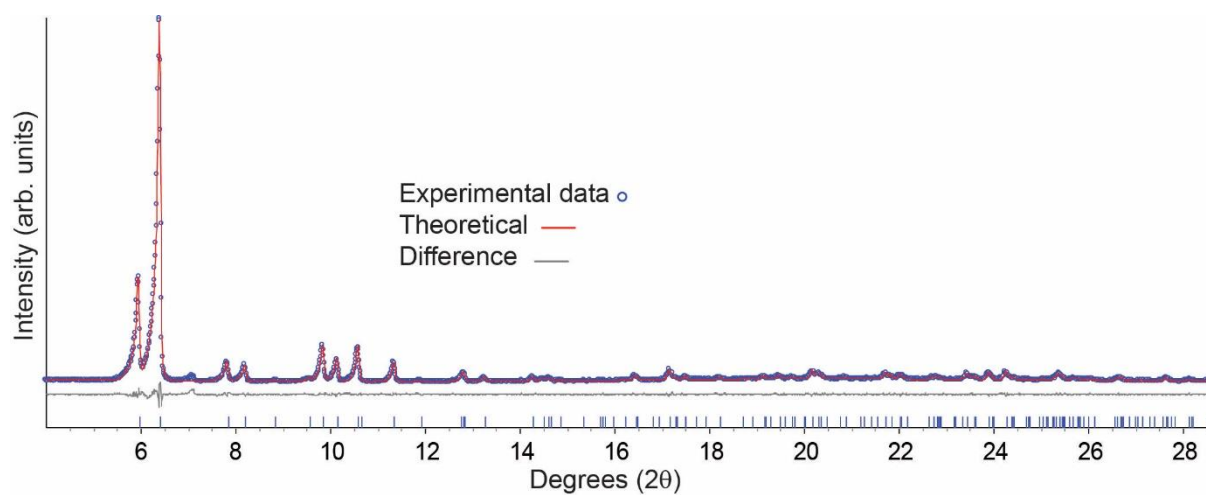


Figure S40. Le Bail refinement of the Powder X-ray diffraction pattern of **UAM-11**. Refinement parameters: $R_p = 6.53$, $R_{wp} = 9.50$, $GoF = 1.34$. Cell parameters $Cmca$, $a = 29.7$; $b = 22.6$; $c = 21.6 \text{ \AA}$. For comparison, the cell parameters of the single crystal X-ray structure: $Cmca$, $a = 29.3$; $b = 22.3$; $c = 21.1 \text{ \AA}$.